

RESEARCH ARTICLE | MARCH 06 2024

## Design and development of a horizontal contact separated (HCS) test setup for measuring the performance of triboelectric nanogenerator for sustainable energy harvesting applications

Shailendra Kumar  ; Rajesh Kumar Jha   ; Prashant Sharma  ; Ankur Goswami  

 Check for updates

*Rev. Sci. Instrum.* 95, 035002 (2024)

<https://doi.org/10.1063/5.0190787>



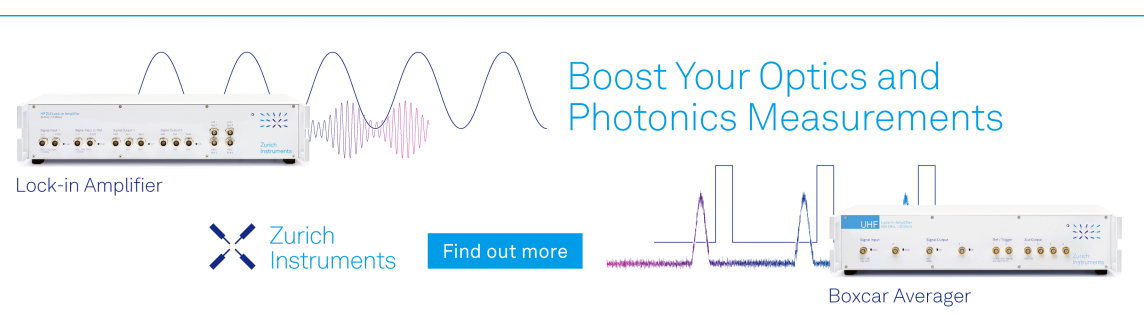
View  
Online



Export  
Citation

CrossMark

06 March 2024 22:06:51



The advertisement features two main products from Zurich Instruments: the UHF Lock-in Amplifier and the Boxcar Averager. On the left, a UHF Lock-in Amplifier unit is shown with several input and output ports. To its right is a graph showing a complex multi-frequency signal being processed by the device. The text "Boost Your Optics and Photonics Measurements" is displayed above the graph. Below the graph, the text "Lock-in Amplifier" is written next to the Zurich Instruments logo, which consists of a stylized 'X' symbol followed by the company name. A blue button labeled "Find out more" is positioned between the two products. On the right side of the advertisement, a Boxcar Averager unit is shown with its own set of input and output ports. To its right is another graph showing a different type of signal, likely a boxcar average output. The text "Boxcar Averager" is written below this graph.

# Design and development of a horizontal contact separated (HCS) test setup for measuring the performance of triboelectric nanogenerator for sustainable energy harvesting applications

Cite as: Rev. Sci. Instrum. 95, 035002 (2024); doi: 10.1063/5.0190787

Submitted: 8 December 2023 • Accepted: 15 February 2024 •

Published Online: 6 March 2024



View Online



Export Citation



CrossMark

Shailendra Kumar,<sup>1</sup> Rajesh Kumar Jha,<sup>1,a)</sup> Prashant Sharma,<sup>2</sup> and Ankur Goswami<sup>1,a)</sup>

## AFFILIATIONS

<sup>1</sup> Department of Materials Science and Engineering, Indian Institute of Technology Delhi, Hauz Khas, New Delhi 110016, India

<sup>2</sup> School of Physics, Indian Institute of Science Education and Research Thiruvananthapuram, Kerala 695551, India

<sup>a)</sup> Authors to whom correspondence should be addressed: [jharajesh@mse.iitd.ac.in](mailto:jharajesh@mse.iitd.ac.in) and [agoswami@mse.iitd.ac.in](mailto:agoswami@mse.iitd.ac.in)

## ABSTRACT

Triboelectric nanogenerators (TENGs) can play a pivotal role in harnessing non-utilized reciprocating motion and convert it into electrical energy that can later be stored in a battery or capacitor to power various Internet of Things-based smart electronic and wearable devices. Herein, we designed a cost-effective instrumental test bed focused on investigating the output performance of a horizontal contact separation mode triboelectric nanogenerator by varying the input parameters, such as applied force, motor speed, triboplate separation, and frequency of instrumental setup. The test bed mainly consists of three major parts: (i) application of force, (ii) tapping of TENG sample, and (iii) output parameters measurement. The output performance in terms of open circuit output voltage ( $V_{OC}$ ), short circuit current ( $I_{SC}$ ), and power density of polydimethylsiloxane-based TENG was monitored and optimized by varying the input parameters. A low-cost current measuring circuitry using an operational amplifier integrated circuit has been proposed with 92% accuracy. The maximum value of  $V_{OC}$  and  $I_{SC}$  was observed to be 254 V and 31.8  $\mu$ A at a motor speed of 600 rpm, the distance between both the plates was 6 mm, the input applied force of 40 N, and the striking frequency of 3 Hz. The maximum power density of 2.1 W/m<sup>2</sup> was obtained at an input impedance of 8 k $\Omega$ . The durability of the test bed as well as the TENG sample was also measured for 25 h. The degree of uncertainty was measured for  $V_{OC}$ ,  $I_{SC}$ , and applied force and calculated to be 1.62%, 7.45%, and 6.27%, respectively.

Published under an exclusive license by AIP Publishing. <https://doi.org/10.1063/5.0190787>

## I. INTRODUCTION

The renewable green energy demand has been growing at a rapid rate over the past few decades due to unprecedented threats of the energy crisis and heavy reliance on fossil fuels.<sup>1</sup> This surge in energy demand can be fulfilled by various sustainable energy sources, such as mechanical vibration energy,<sup>2</sup> tidal energy,<sup>3</sup> wind energy,<sup>4</sup> biofuel,<sup>5</sup> and so on. Particularly, after the emergence of the Internet of Things (IoT)-based devices, these omnipresent non-conventional mechanical energy sources can perfectly be utilized as the power source for different sensors.<sup>6,7</sup> Being able to harvest mechanical energies, various kinetic energy harvesters with a transduction mechanism that can convert electrostatic,<sup>8</sup> electromagnetic,<sup>9</sup> pyroelectric,<sup>10</sup> and triboelectric<sup>11</sup> into electrical energy.

Among the above-mentioned energy harvesting mechanisms, the triboelectric nanogenerator (TENG) with its significant advantages, such as simple fabrication, lightweight, toxicity-free, and ability to harvest energy at very low frequency(<4 Hz),<sup>12,13</sup> has drawn immediate interest.

The IDTechEx report suggests that by 2030, triboelectric nanogenerators could surpass piezoelectric energy harvesters in terms of power enhancement, ranging from milliwatts to watts.<sup>14</sup> The triboelectric nanogenerator operates by harnessing the combined effects of triboelectrification and electrostatic induction, enabling the conversion of mechanical energy into electrical energy. TENGs mainly work in four modes: (i) contact separation mode, (ii) sliding contact mode, (iii) single electrode mode, and (iv) freestanding triboelectric layer mode.<sup>15</sup> In the contact separation mode, two different

triboelectric materials contact each other after applying external mechanical force. Friction between two triboelectric material films creates oppositely charged surfaces. Once the two surfaces are separated by a small gap, a potential drop is created by removing the external force, and the charge transfer occurs between two electrodes.<sup>16,17</sup> The contact separation mode working mechanism is carried out in three stages: (i) charge generation, (ii) charge separation, and (iii) charge flow.<sup>18</sup> Many research groups have been working to improve the efficiency, power, and charge density of TENG devices by the effective use of impact forces, surface morphology, contact area, and micro and nanocrystal structure engineering of materials.<sup>19–22</sup> Various studies have been carried out to investigate the effect of force by applying finger tapping, hand motion, walking, running, and so on, which indeed found not suitable to find actual force.<sup>23–25</sup> There are several operational parameters, such as impact force, and tapping frequency, which are required to be precisely controlled during manual tapping. Therefore, the precise control of experiments demands the control of these operational parameters. However, it is difficult to measure the actual force in real-time when the two surfaces come in contact with each other as the sensor element (force sensor) has to be mounted between these two surfaces.

Up until now, monitoring the performance of the TENG device has mostly been carried out by the nonquantitative measurement methods, such as finger tapping, foot movement (inputs), and LED blinking (output), which do not reflect the actual measurements during real-time experiments.<sup>26</sup> Earlier, various vibration shakers, often used to characterize the piezoelectric harvester, have been employed to apply input force to the TENG devices in order to characterize their performance.<sup>27–29</sup> The frequency and magnitude of force applied in such cases were majorly controlled by function generators.<sup>23</sup> Later on, the precise control of force was carried out using a computer-programmed stepper motor. Hong *et al.*<sup>30</sup> reported the triboelectric nanogenerator experimental setup that operates in a contact mode with the capability of real-time measurements of force, speed, current, and voltage. However, the estimated cost of such setups based on equipment and accessories used was around USD 11 000–16 500.<sup>31–33</sup> Normally, the output current generated from TENG devices varies in the range of nano to milli amperes, which is often measured using various low noise amplifiers costing around USD 2600.<sup>34</sup> Recently, Sharma and Agarwal measured the output current and voltage using a Pico scope for vertical contact-separated TENG setup.<sup>35</sup> Hence, there is a need for a low-cost test setup that can measure real-time output parameters with high durability. The instrumental issues can be mitigated by regularly recalibrating the instrument. In addition to the instrumental setup constraints, the TENG may also suffer from various other factors, such as limited material availability, mechanical wear and tear, sensitive to environmental conditions (i.e., temperature, ambient gas, humidity), contact resistance, scale up challenges with maintaining the power density, efficiency, and reliability, and narrow operational frequency range. To mitigate these above-mentioned issues, the TENG devices can be fabricated by taking materials with consistent properties and carrying out the experiment in a controlled environment with temperature and humidity sensors. The TENG sample can be regularly checked for mechanical wear and tear. The contact resistance can be minimized through proper material selection, surface treatment, and maintaining consistent contact pressure. The appreciable

amount of power density can be achieved by optimizing TENG input parameters (impact force, frequency, contact area, and input impedance).

In this work, we have developed a low-cost instrumental test setup for measuring tribocharges named the Horizontal Contact Separation Mode Triboelectric Nanogenerator (HCS-TENG). The instrument not only measures the charges due to triboelectrification when two dissimilar materials come into contact but is also designed in such a fashion that it will allow to investigate the generation of the charges due to the synergistic effect of photovoltaic and triboelectricity. Here, the TENG sample was prepared using polydimethylsiloxane (PDMS) and copper as a triboelectric material. The fabricated TENG was tested using in-house built HCS-TENG and the main objective was to obtain maximum voltage, current, and power density by varying different instrumental parameters, such as speed, force, frequency, and surface area of TENG.

## II. EXPERIMENTAL SETUP AND WORKING MECHANISM

We have designed an experimental setup that incorporates a tapping system for the controlled application of mechanical energy to the device under study. In addition, the setup includes a measurement system capable of quantifying the impact force, frequency, and output performance of the device. The schematic block diagram of the in-house developed horizontal contact separation mode TENG's performance measurement setup is shown in Fig. 1. The experimental setup mainly comprised of programmable logic controller (PLC), PLC driver, servo motor, shaker, primary plate, secondary plate, TENG device, oscilloscope, Keithley source meter, and load cell with the display unit.

The complete TENG performance measurement instrumental setup has been placed on a rectangular base plate made up of cast iron having a thickness of around 1.0 cm and a total area of 1500 cm<sup>2</sup> capable of absorbing various environmental disturbances and vibrations caused by motion of other components (mainly servo motor). The insulating material is coated on the base plate to avoid conduction through the metal plate. An ac servomotor (Panasonic) working in a closed-loop feedback mechanism can operate with high efficiency and accuracy using PLC, which allows us to control and

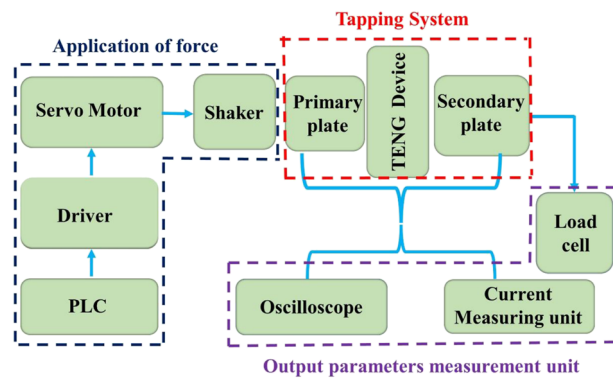


FIG. 1. Schematic diagram of the in-house developed instrumental setup to measure the output performance of TENG.

regulate the speed of rotation, linear motion, or shaft movement.<sup>36</sup> Furthermore, it also transmits commands related to position, velocity, and torque control to the servo driver, which is connected to the servo motor. The steel support rod is then attached to the substrate holder or primary/secondary plates, serving the purpose of providing stability for both the moving and stationary substrate holders. The shaft and bearing are linked to a linear ball screw, enabling movement in both inward and outward directions. In addition, a load cell is attached to the rear side of the stationary substrate holder to measure the real force that can exert up to 400 N when the primary substrate holder impacts the secondary plate.

The whole instrumental setup is monitored and controlled by the user through an INVT display. In order to investigate the impact of the photovoltaic effect on triboelectricity, additional attachments, such as diode laser and laser mount, have been mounted on the back side of the secondary plate as shown in Fig. 2 (item 7). The design

of the instrument is scalable according to its application at micro or macrolevel and the TENG sample to be attached. This work demonstrated the result of the PDMS-based TENG device of surface area ( $2 \times 2 \text{ cm}^2$ ). The proposed instrumental setup with the existing components is capable to handle TENG samples having a surface area of  $10 \times 10 \text{ cm}^2$ . If we consider the TENG sample with a large surface area greater than ( $10 \times 10 \text{ cm}^2$ ) for a smart shoe or shoe sole with a human motion monitoring application, it would require scaling up the TENG sample holding plate. Furthermore, as the TENG sample size increases the load-bearing capacity of the servo motor and ball screw, the other mechanical components need to be enhanced.

The different triboelectric materials can be attached to the primary and secondary plates to measure the electrical output performances with different materials configurations, such as polymer-polymer, polymer-metal, metal-semiconductor, and so on.<sup>37</sup> Figure 2 (multimedia available online) depicts the in-house

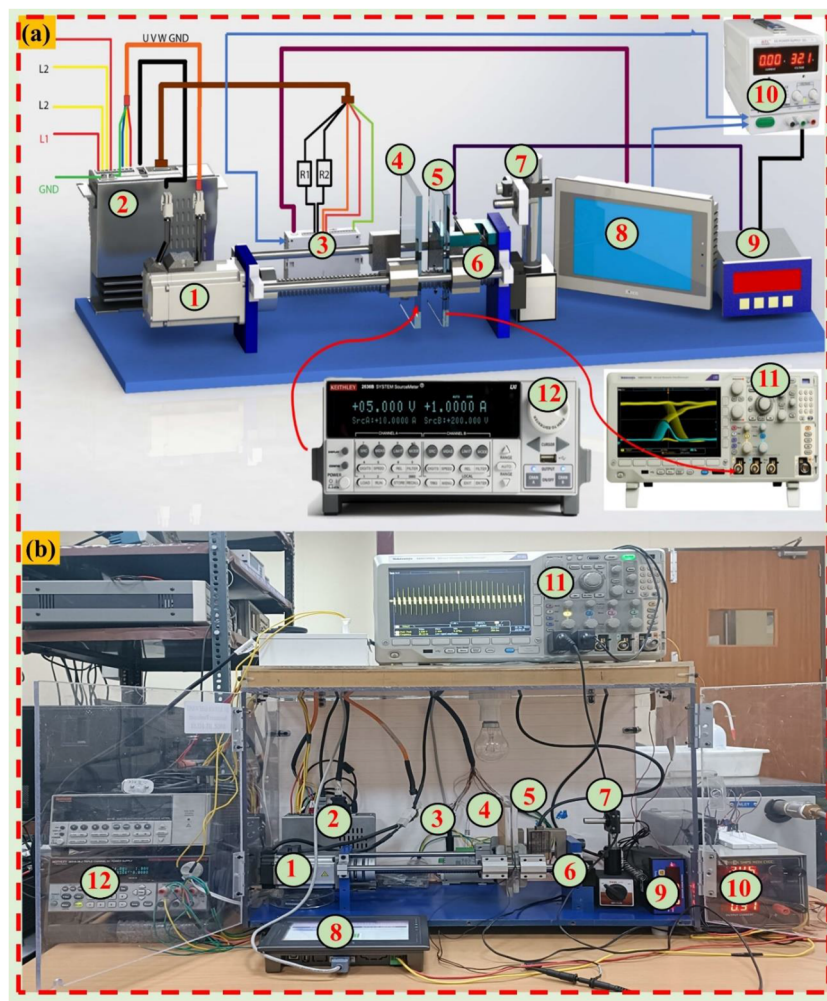


**FIG. 2.** Instrumental setup. (a) Schematic and (b) pictorial view, in which (1) servo motor, (2) servo driver, (3) PLC, (4) primary plate (moving), (5) secondary (stationary) plate, (6) load cell, (7) laser source, (8) controller display, (9) load display unit, (10) 20–24 V power supply, (11) oscilloscope, and (12) Keithley source meter. Multimedia view available online.

built HCS-TENG experimental setup that mainly consists of three sections in terms of operation: (a) application of force, (b) tapping system of TENGs, and (c) output parameters measurement unit.

### A. Application of input force

In the case of TENG devices, the output of the device majorly depends on the magnitude of the impact force exerted on the two triboelectric layers attached to the primary (item 4) and secondary (item 5) plates as shown in Fig. 2. To report the efficiency of the device, it is important to know the magnitude of the force applied to these triboelectric layers. Hence, in order to characterize the TENG devices, it is indispensable to exert and measure the force for operating the in-house developed HCS-TENG instrument. To apply this force on the TENG devices, the tribolayer attached to the primary plate has to strike the secondary plate with a sufficient impact. Such ramification is only possible through the horizontal movement of the primary plate, mounted on the ball screw that is attached to the servomotor through the shaft, which strikes hard to the secondary plate. The entire back and forth linear motion of the primary plate is governed by the servomotor that is controlled by PLC and servo driver.

It is important to note that the linear servo motor along with its driver operates at 220 V AC power supply, while a separate 24 V DC power supply is required to power the PLC.

### B. Tapping system

HCS-TENG instrument utilizes the impact force to establish contact between the primary plate (substrate holder) and the secondary plate (substrate holder). These plates or substrate holders, referred to as vibrating plates, are positioned perpendicular to the direction of motion. The tapping system functions in a horizontal manner, with variable speeds and distances to cater to user-specific requirements. Through tapping, it produces diverse frequencies and impact forces that can be finely tuned to generate detectable electrical signals. These electrical signals are subsequently captured and measured by an electrical measurement system.

### C. Output parameters measurement unit

The magnitude of input applied force within the TENG instrument is being measured by an S-type load cell procured from M/s.

Synopsis Techno Instruments. It is suitable for measuring both compressive and tensile forces greater than 400 N. The load cell is connected to an indicator that provides real-time measurements, allowing immediate access to the actual data. To facilitate data recording and display, a load cell display unit is connected to the load cell. This display unit operates with a 24 V DC power supply and is responsible for recording the measured data and presenting it in a clear and understandable manner, ensuring efficient monitoring and analysis. For the measurement of triboelectrical output parameters, such as output voltage ( $V_{OC}$ ) and short circuit current ( $I_{SC}$ ), a Keithley source meter (2636 B) is used in real-time. Given that the output current of the TENG is typically very low, in the range of nano ampere to a few microamperes,<sup>38</sup> we measure the output current using a self-written Python program. The current was also measured using an external current measuring circuit made using IC LMC6001.

## III. SYSTEM CONFIGURATION

The design of the HCS-TENG instrument setup has been focused on three key points: (i) the ability to adjust the two contact surfaces horizontally to ensure complete overlap, (ii) to maintain the parallelism between the triboelectric material surfaces to avoid local contact, and (iii) real-time measurement of all input as well as output parameters as depicted in Figs. 3–5. The proposed setup includes a one-axis horizontal stage and an s-type load cell force/torque sensor, as depicted in Fig. 2. One end of the sample is fixed to the s-type load sensor, while the other end is placed on a rotating lead screw perpendicular to the linear motor's direction.

The one-axis horizontal stage enables precise horizontal positioning. The s-type load sensor functions in both tension and compression modes. For accurate measurement of the output voltage and current generated by the contact-mode TENG, a low-noise current amplifier (Keithley 2636B source meter & oscilloscope) instrument is employed, capable of measuring currents and voltages at the pico level. In addition, an oscilloscope with a high-voltage measurement range of up to 400 V is used to measure peak-to-peak voltage. The system components are controlled, and experimental data are recorded in real-time. The system starts working after installing the TENG samples on the primary and secondary plates. Both the plates were kept separated at a distance "d," which continuously changes after the application of force or movement of plates.

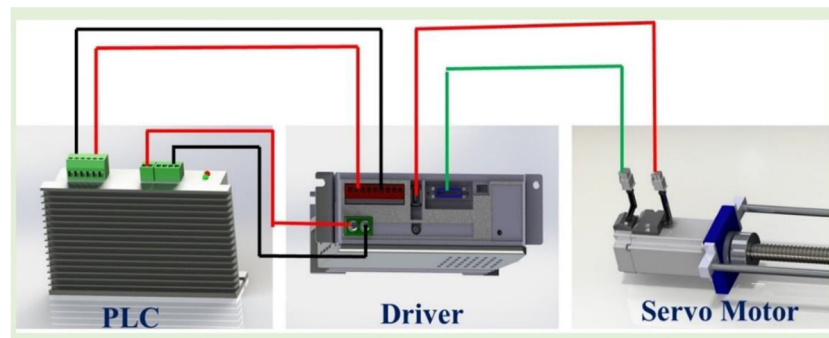
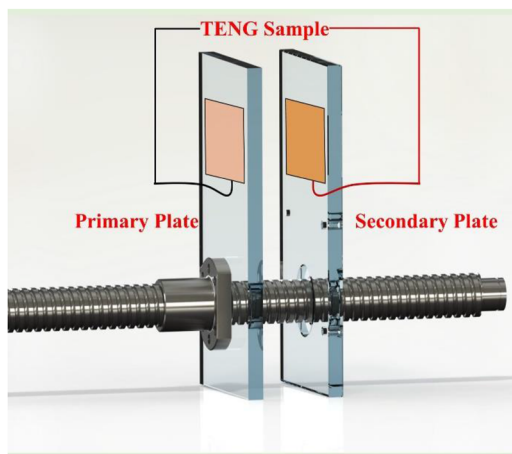


FIG. 3. Schematic of a TENG device controlled by PLC and driver.



**FIG. 4.** Schematic presentation of the tapping system of the TENGs device with primary plate (moving) and secondary plate (stationary).

The corresponding output parameters are being measured using different equipment. The process flow of working of triboelectric setup is shown in Fig. 6. The key components, such as servo motor with PLC, load cell, oscilloscope, and source measuring unit, were calibrated before carrying out the experiment. In addition, the ambient temperature during the experiment was kept constant, although the humidity might have varied by  $\pm 5\%$ .

#### IV. TENG SAMPLE PREPARATION

To measure the performance of the instrument, the TENG test sample was prepared using polydimethylsiloxane (PDMS) and copper as primary and secondary triboelectric material layers. PDMS was deposited using a spin coater at a rotating speed of 1000 rpm for 2 min and post-deposition baking was carried out at  $80^\circ\text{C}$  for 2 h. The spin-coated 500  $\mu\text{m}$ -thick PDMS film was attached to a copper electrode, as shown in Fig. 7.

#### V. TRIBOELECTRIC CHARACTERIZATION DETAILS

The TENG sample was subjected to the instrumental test setup to obtain various triboelectrical output parameters, such as open

circuit voltage ( $V_{oc}$ ), short circuit current ( $I_{sc}$ ), and output power density. The measurements were carried out at different tapping frequencies ranging from 0.5 to 5.0 Hz to correlate the obtained results with human motions, such as walking, jogging, running, jumping, hand tapping, and hand movement. The magnitude of applied input force was also varied from 1 to 60 N.

In the experimental section, we used an oscilloscope (MDO 3024) with four input channels (channel A) and a Keithley 2636B source meter in the measurement setup. The TENG device output has been connected with channel A and the source meter provides measured real-time electrical parameters.

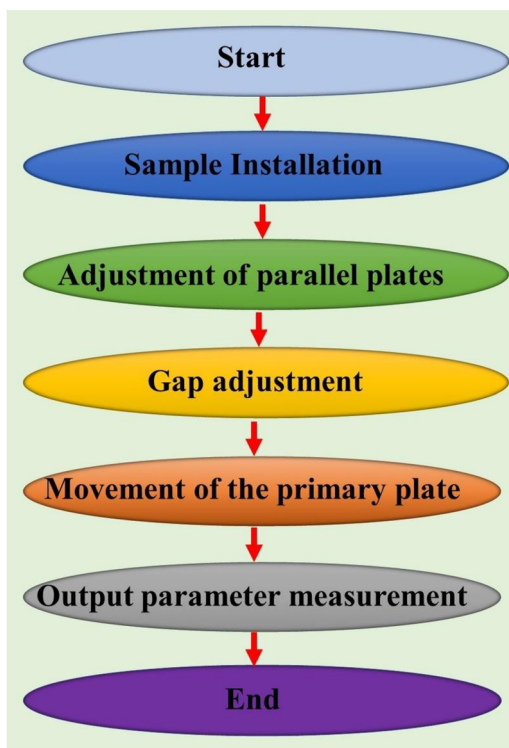


**FIG. 6.** Performance evaluation procedure using the contact separation mode.

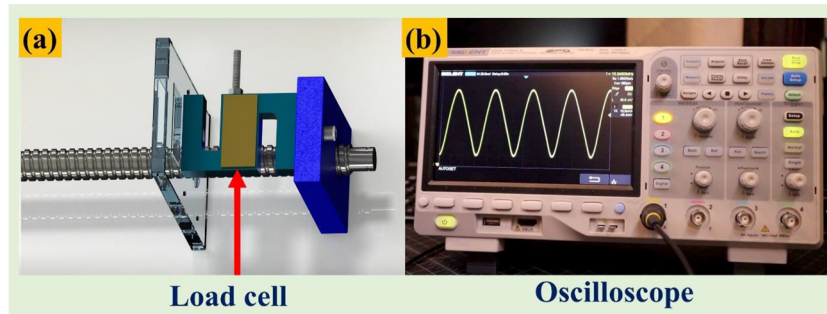


**FIG. 5.** Output performance parameter measurement unit: (a) force measurement using loadcell and (b) voltage measurement using an oscilloscope.

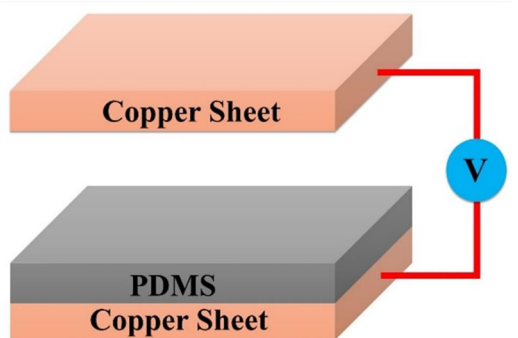


FIG. 7. Triboelectric nanogenerator (TENG) sample.

## VI. RESULTS AND DISCUSSIONS

### A. Triboelectric characterization

The fabricated TENG samples were fixed in an instrumental setup to monitor its output performance. The primary or moving plate is attached with copper clad, which acts as primary electrodes, and secondary electrode comprises of PDMS thin film on the copper electrode. The PDMS thin film had a thickness of  $500\ \mu\text{m}$  and the contact surface area of  $4\ \text{cm}^2$ . The relative dielectric constant of PDMS was found to be  $2.0\text{--}2.25$ .<sup>39</sup> All the experimental procedures were carried out under standard room temperature conditions ( $30^\circ\text{C}$ ) with a humidity level of 30%. Initially, an input force was applied at different speeds or frequencies, and corresponding output parameters ( $V_{\text{OC}}$  and  $I_{\text{SC}}$ ) were measured and shown in Fig. 8. The distance between both the plates was also varied in 2, 4, 6, 8, and 10 mm. This analysis provides valuable insights into the effect

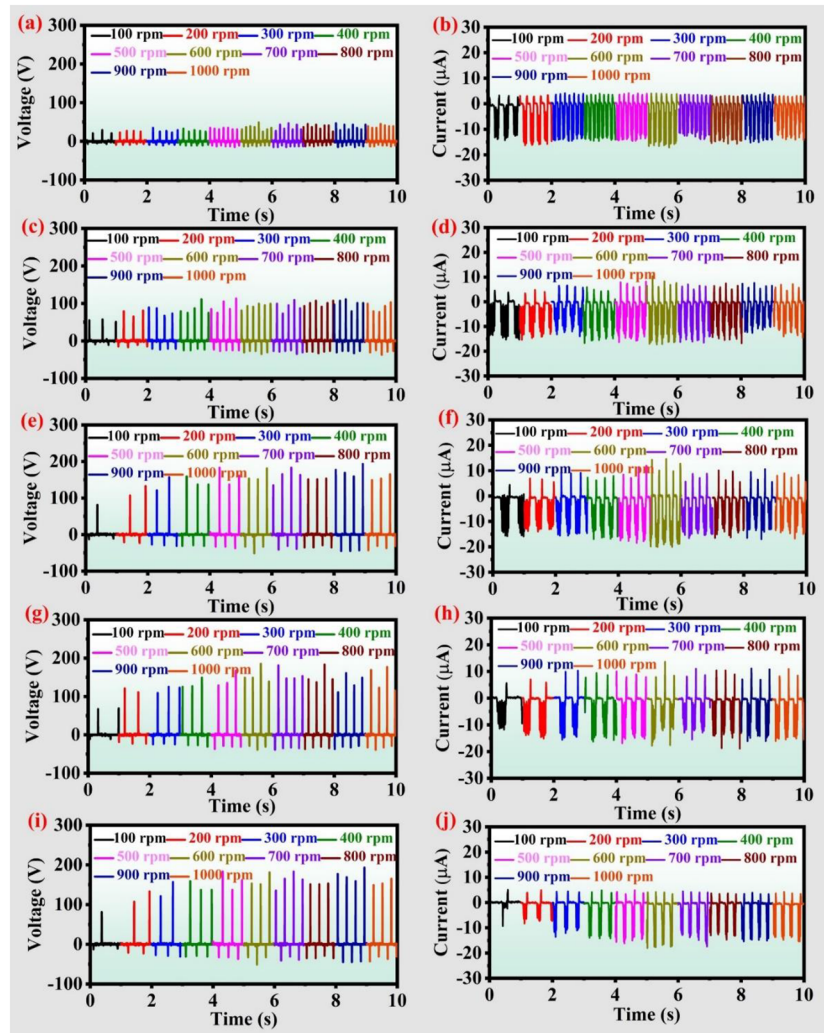


FIG. 8. Open-circuit voltage ( $V_{\text{OC}}$ ) and short-circuit current ( $I_{\text{SC}}$ ) having a separation distance between the two parallel plates of (a) and (b) 2 mm (c) and (d) 4 mm (e) and (f) 6 mm, (g) and (h) 8 mm, and (i) and (j) 10 mm.

of variation in the distance between the plates, contact area, and speed of the motor on the triboelectric output performance parameters. The  $V_{OC}$  and  $I_{SC}$  were observed to be maximum (254 V and 31.79  $\mu$ A) at the motor speed of 600 rpm when the distance between both the triboplates was fixed at 6 mm.

The motor speed was varied from 100 to 1000 rpm in the step size of 100 rpm and corresponding  $V_{OC}$  and  $I_{SC}$  were measured at different separating distances (2, 4, 6, 8, and 10 mm) and shown in Fig. 8. At a fixed distance (i.e., 2, 4, 6, 8, and 10 mm), by varying the motor speed from 100 to 600 rpm, the  $V_{OC}$  and  $I_{SC}$  increase steadily as evident from Figs. 8(a)–8(j); further increase in the speed of motor causes no change in  $V_{OC}$  rather decrease in  $I_{SC}$  was observed. This decrease in  $I_{SC}$  may be due to the less impact of applied force on the contact area of the triboelectric plate.

The effect of varying the motor speed and corresponding change in  $V_{OC}$  and  $I_{SC}$  are shown in Figs. 9(a) and 9(b), and instantaneous power is tabulated in Table I. The optimized input parameters are highlighted (with bold font). The impact of applied force during contact on the  $V_{OC}$  and  $I_{SC}$  was further investigated, and the obtained results are shown in Figs. 9(c) and 9(d). The TENG device demonstrated a relationship between contact force and its output voltage and short-circuit current. Initially, increasing contact force resulted in a rise in  $V_{OC}$  and  $I_{SC}$ , peaking at 40 N.

**TABLE I.** Experimentally measured TENG results with different parameters. Boldface indicates optimized input parameters.

S.No.	Speed (rpm)	Frequency (Hz)	$V_{Peak}$ (V)	$I_{Peak}$ ( $\mu$ A)	$P_{Inst}$ (mW)
1	100	0.5	102	18.30	1.86
2	200	1.0	180	19.38	3.48
3	300	1.5	202	22.88	4.62
4	400	2.0	214	24.67	5.27
5	500	2.5	238	26.04	6.19
6	<b>600</b>	<b>3.0</b>	<b>254</b>	<b>31.79</b>	<b>8.07</b>
7	700	3.5	238	26.38	6.27
8	800	4.0	248	25.80	6.39
9	900	4.5	248	24.37	6.04
10	1000	5.0	242	23.82	5.76

However, further increments in contact force caused a no change in  $V_{oc}$  and decrease in  $I_{sc}$ . This behavior can be attributed to the no change in the charge carrier concentration of the TENG sample beyond a point.<sup>40</sup> With low contact force, the roughness led to non-uniform contact, resulting in inconsistent output. As

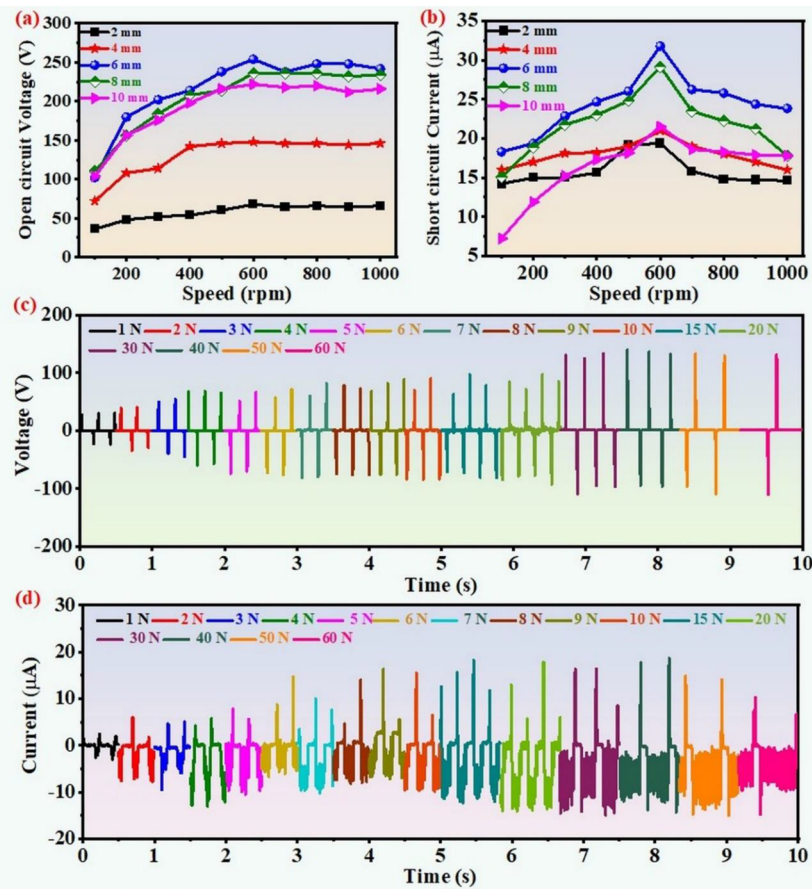


**FIG. 9.** Open-circuit voltage at (a) different speeds (100–1000 rpm), and (c) force (1–60 N) and short circuit current at (b) different speeds and (d) different forces (1–60 N).

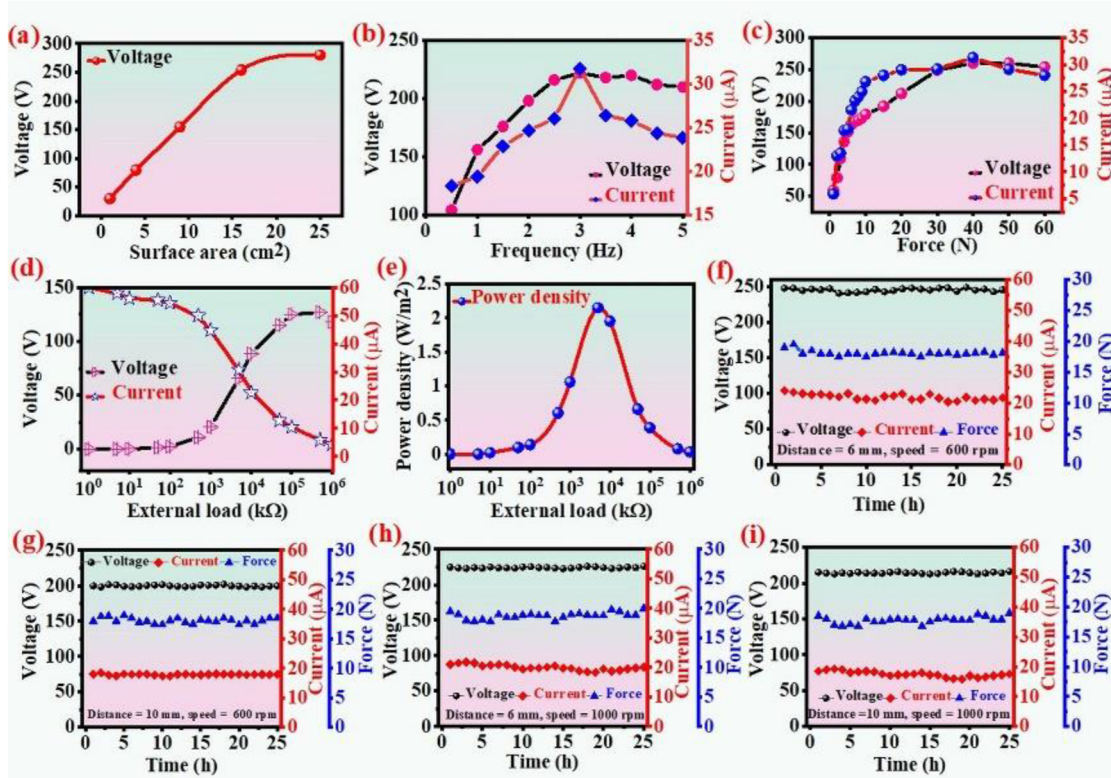


**FIG. 10.**  $V_{OC}$  and  $I_{SC}$  variation with respect to (a) surface area (b) frequency, (c) force, (d) external resistive load, (e) power density vs load, and durability test for  $V_{OC}$ ,  $I_{SC}$ , and force, (f) distance = 6 mm and speed = 600 rpm, (g) distance = 10 mm and speed = 600 rpm, (h) distance = 6 mm and speed = 1000 rpm, and (i) distance = 10 mm and speed = 600 rpm.

the contact force surpassed a threshold, overall contact was established, leading to output stabilization. Consequently, excessively high contact forces had minimal impact on the TENG device's output.<sup>41</sup> Through analyzing the connection between contact force and corresponding changes in output voltage and short circuit current, valuable insights into the optimal contact force for achieving desirable TENG performance were obtained.

The peak-to-peak open circuit voltage, short-circuit current, and instantaneous power were measured with respect to surface area, motor speed, and frequency. The peak-to-peak  $V_{OC}$  increases as the contact surface area increases, as shown in Fig. 10(a).

The increase in the contact surface area allows the generation of more number of charge carriers on the surfaces of triboelectric materials upon contact with each other. The increase in  $V_{OC}$  varies linearly with respect to surface area up to  $16\text{ cm}^2$ , and further increase in the surface area does not cause significant improvement in  $V_{OC}$  due to non-uniform application of impact force on larger area. Figure 10(b) presents the correlation between  $V_{OC}$  and  $I_{SC}$  with different frequencies of a linear servo motor, ranging from 1 to 5 Hz. Notably, the highest values for both  $V_{OC}$  and  $I_{SC}$  were observed at a specific frequency of 3 Hz. At frequencies lower or higher than 3 Hz,  $V_{OC}$  and  $I_{SC}$  exhibited relatively no change or lower values. Figure 10(c) depicts the relationship between output parameters ( $V_{OC}$  and  $I_{SC}$ ) and varying forces, ranging from 1 to 60 N. The voltage and current

concerning different external load resistances ( $1\Omega$  to  $1\text{ M}\Omega$ ) were measured and shown in Fig. 10(d). The maximum power density of  $2.1\text{ W/m}^2$  was obtained at an input impedance of  $8\text{ k}\Omega$  as shown in Fig. 10(e).

The power density varies with the external resistive load applied to the circuit; according to the maximum power transfer theorem, the maximum power transfers to the load when applied external load resistance is equal to the input impedance. Hence, at  $8\text{ k}\Omega$ , the maximum power density was obtained. In order to assess the degree of uncertainty or durability of instrumental setup, measurements were performed for 25 h to observe  $V_{OC}$ ,  $I_{SC}$ , and impact force at an interval of 60 min. The obtained average peak-to-peak  $V_{OC}$  and  $I_{SC}$  were

**TABLE II.** Durability test under different input conditions.

Input parameters		Testing parameters		
Distance (mm)	Speed (rpm)	Force (N)	$V_{OC}$ (V)	$I_{SC}$ ( $\mu\text{A}$ )
6	600	19–18	250–247	26–25
10	600	18–19	205–200	19–18
6	1000	21–20	225–223	20.5–20
10	600	18–19	221–218	19–18

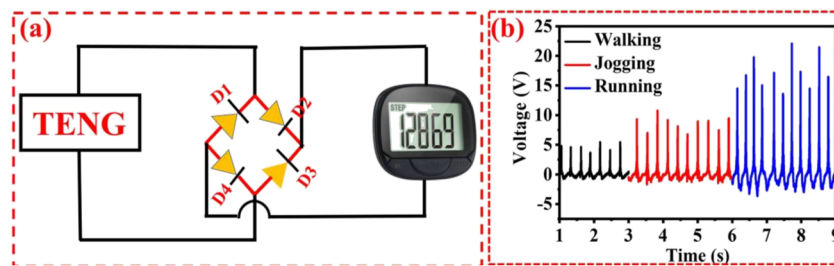


FIG. 11. Application of TENG in (a) powering a pedometer and (b) generating signals during human motion.

plotted in Figs. 10(f)–10(i) and found to vary between 245 and 254 V and 25–26  $\mu$ A, respectively, with the applied force variation from 19 N to 1 N. The standard deviation of the measured data was 2.27, 2.68, and 2.19, respectively. The degree of uncertainty was measured for  $V_{OC}$ ,  $I_{SC}$ , and applied force and measured to be 1.62%, 7.45%, and 6.27%, respectively. The durability test was also carried out under different input parameter conditions mentioned in Table II.

## VII. APPLICATION OF TENG

The PDMS-TENG was utilized in powering the pedometer that counts the human steps. The fabricated device was also used as a human motion sensor that generates the voltage signal during a human walk, jog, and run, as shown in Fig. 11.

## VIII. COST ESTIMATION

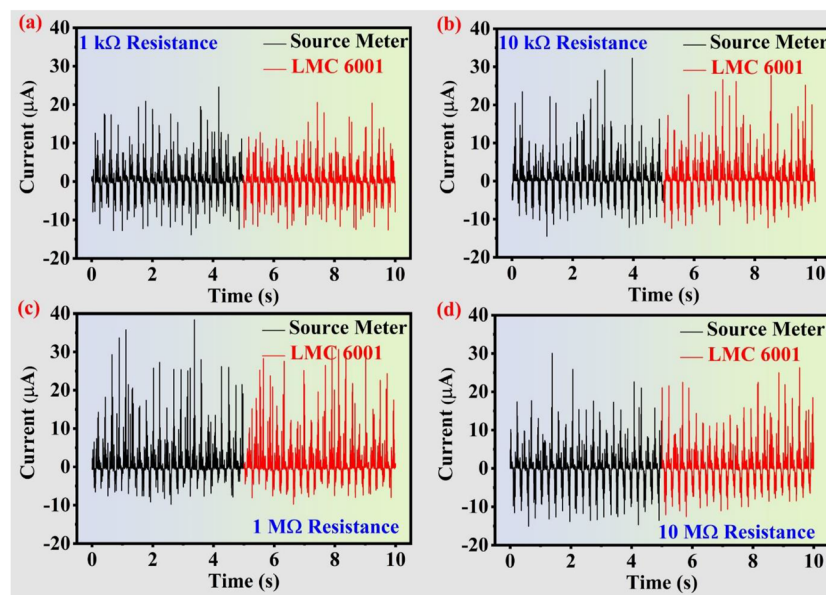
### A. Current measuring unit

Generally, the short-circuit output current ( $I_{SC}$ ) has been measured using the Keithley 2636B source meter that costs around USD 2900. Hence, the current measurement circuit using an

instrumentation amplifier IC was proposed, which measures the current in terms of voltage and being shown on an oscilloscope. The schematic diagram of the current measuring unit (CMU) made using the integrated circuit having code LMC6001 and 1 M $\Omega$  resistor, as shown in Fig. S1 (see the supplementary material). The TENG input is applied to one of the terminals (inverting) of the amplifier, and the amplified output voltage is fed to an oscilloscope to measure the voltage.

TABLE III. Comparison of electrical currents measured using the source meter and LMC6001 at different load resistances.

Load resistance	Peak current measured by source meter ( $\mu$ A)	Peak current measured by LMC6001 ( $\mu$ A)	% Difference
1 k $\Omega$	35.00	32.00	8.5
10 k $\Omega$	44.10	41.40	6.1
1 M $\Omega$	43.62	40.82	6.4
10 M $\Omega$	42.55	39.85	6.3

FIG. 12. Output current measured by the source meter and LMC6001-based circuit at different load resistances of (a) 1 k $\Omega$ , (b) 10 k $\Omega$ , (c) 1 M $\Omega$ , and (d) 10 M $\Omega$ .

**TABLE IV.** Estimated costs of the electrical and mechanical components used to build HCS-TENG instrumental setup.

S. No.	Name of equipment	Cost (USD)
1	Linear servo motor (Panasonic MHMJ042P1U 400 W 24 V DC)	128
2	MBDJT2210 LIQI series servo motor driver	146
3	Microcontroller	39
4	30 V at 3 A SMPS power supply	61
5	Aluminum flexible coupling	9
6	Shaft and bearing KP008	12
7	Steel linear rod (8 mm)	9.76
8	Acrylic sheet (10 mm) primary plate	0.61
9	Acrylic sheet (10 mm) secondary plate	0.61
10	SYNAPSIS load cell and indicator	30.50
11	INVT display	61
12	Cast iron (10 mm thickness) base plate	6.10
13	Digital oscilloscope	674.84
14	Current measuring system (LMC 6001)	28.06
<b>Total</b>		<b>1206.48</b>

The TENG output is fed to the input inverting terminal of the circuitry, which had a sensitivity of  $10 \mu\text{A}/\text{V}$  and a voltage slew rate of  $1.6 \text{ V}/\mu\text{s}$ .

The current measured using a source meter and LMC6001 is tabulated in [Table III](#). The current measured at different external

load resistances is shown in [Fig. 12](#). The measured difference between the source meter and LMC6001 varies from 6.1% to 8.5%.

The cost (highlighted in bold font) associated with all the required electrical and mechanical components used in the construction of the HCS-TENG instrumental test bed is

**TABLE V.** Estimated cost comparison of components required for the reported conventional experimental setup.

S.No.	Instrument working mode	Key components	Overall cost (USD)	References
1	Vertical contact	Linear power amplifier, shaker, force sensor, signal conditioner, digital phosphor oscilloscope, input module, electrometer, function generator	16 260.0	<a href="#">31</a>
2	Vertical contact	Signal generator, picoammeter, digital oscilloscope, vibration shaker	13 684.0	<a href="#">32</a>
3	Horizontal contact	Low-noise DC driver, low-noise current amplifier, electrometer (Keithley 6517B), voice coil actuator, capacitive displacement sensor, digital signal processing-based real-time controller	16 000.0	<a href="#">30</a>
4	Horizontal contact	Low-noise current amplifier, system electrometer, linear motor	11 982.0	<a href="#">33</a>
5	Vertical contact	Mechanical body, power supply, lab jack, load cell with an amplifier, switching power supplies isolated AC-DC 12 V DC 4.2 A for I-to-v, pico scope 3206D MSO	2 598.58	<a href="#">35</a>
6	Horizontal contact	Linear servo motor (Panasonic MHMJ042P1U 400 W 24 V DC), MBDJT2210 LIQI series servo motor driver, microcontroller, 30 V at 3 A SMPS power supply, SYNAPSIS load cell and indicator, INVT display, digital oscilloscope Tektronix, current measuring system (LMC6001)	1 206.48	In this paper

mentioned in Table IV. The cost of the overall setup was found to be USD1206.48, which is very much less than the various other conventional setups having cost ranging from USD 11 000–15 000. The detailed comparison along with this study (highlighted in boldface) is given in Table V. The comparison clearly demonstrates that the proposed experimental setup offers a significantly lower cost alternative to conventional setups.

## IX. CONCLUSIONS AND FUTURE SCOPE

In this study, we have demonstrated the design of the cost-effective HCS-TENG instrumental test setup to monitor the output performance by optimizing the input parameters, such as applied force, frequency, and separation between triboplates. The overall cost of the in-house built setup is around USD 1206.48. The PDMS-based TENG sample was fabricated, and its triboelectric output parameters ( $V_{OC}$  and  $I_{SC}$ ) were measured with respect to the controlled variation of instrumental input parameters. The maximum value of  $V_{OC}$  and  $I_{SC}$  was found to be 254 V at 40 N and 31.79  $\mu$ A at 40 N, maintaining the motor speed constant at 600 rpm, the distance between both the plates was 6 mm, and the striking frequency of 3 Hz. A low-cost current measuring circuit was also developed to measure  $I_{SC}$ . This in-house built test bed setup is capable of measuring the performance of horizontal contact-separation mode TENGs. In the future, this instrumental setup can be modified for three-axis movements (horizontal, vertical, and inclined) by including the slider crank mechanism. It can be transformed into a sensing setup that can sense ambient gases, temperature, and pressure. The study of various parasitics (capacitance and inductance) is to be done to maximize the power output.

## SUPPLEMENTARY MATERIAL

See the supplementary material for the current measuring circuit.

## ACKNOWLEDGMENTS

This work was supported by the Start-up Research Grant [No. SRG-(2019/001984)] SERB-DST, SEED Grant (PLN12), FIRP, and MFIRP Grant of IIT Delhi. This experiment was carried out in the Advanced Electronics Materials and Systems (AEMS) Laboratory, Department of Materials Science and Engineering, IIT Delhi.

## AUTHOR DECLARATIONS

### Conflict of Interest

The authors have no conflicts to disclose.

### Author Contributions

**Shailendra Kumar:** Conceptualization (lead); Data curation (lead); Formal analysis (lead); Investigation (equal); Methodology (equal); Validation (equal); Visualization (equal); Writing – original draft (lead). **Rajesh Kumar Jha:** Conceptualization (equal); Data curation (equal); Formal analysis (equal); Investigation (equal); Supervision (equal); Writing – original draft (equal). **Prashant Sharma:** Formal analysis (supporting); Investigation (equal); Methodology

(equal). **Ankur Goswami:** Conceptualization (equal); Data curation (equal); Formal analysis (equal); Funding acquisition (lead); Investigation (equal); Methodology (equal); Project administration (lead); Resources (equal); Software (equal); Supervision (lead); Validation (equal); Visualization (equal); Writing – original draft (equal).

## DATA AVAILABILITY

The data that support the findings of this study are available within the article.

## REFERENCES

- <sup>1</sup>C.-W. Su, L.-D. Pang, M. Qin, O.-R. Lobonç, and M. Umar, *Energy* **274**, 127304 (2023).
- <sup>2</sup>H. Liu, H. Fu, L. Sun, C. Lee, and E. M. Yeatman, *Renewable Sustainable Energy Rev.* **137**, 110473 (2021).
- <sup>3</sup>M. B. Walsh, *Villanova Environ. Law J.* **19**, 193 (2008).
- <sup>4</sup>Z. Ren, L. Wu, Y. Pang, W. Zhang, and R. Yang, *Nano Energy* **100**, 107522 (2022).
- <sup>5</sup>L. Hassanpourmoghadam, B. Aminzadeh Goharrizi, A. Torabian, E. Bouteh, and B. E. J. B. Rittmann, *Biomass Bioenergy* **169**, 106692 (2023).
- <sup>6</sup>A. Matin Nazar, K.-J. I. Egbe, and P. J. E. T. Jiao, *Energy Technol.* **10**(6), 2200063 (2022).
- <sup>7</sup>P. Jiao, A. Matin Nazar, K.-J. I. Egbe, and A. J. S. E. T. Rayegani “Magnetically circular layers triboelectric nanogenerators (MCL-TENG) for velocity sensing and damage detection,” *Sustainable Energy Technol. Assess.* **53**, 102644 (2022).
- <sup>8</sup>D. Zhu and S. Beeby, *Energy Harvesting Systems: Principles, Modeling Applications* (Springer, 2011), pp. 1–77.
- <sup>9</sup>M. A. Halim, H. Cho, and J. Y. Park, *Energy Convers. Manage.* **106**, 393 (2015).
- <sup>10</sup>M. Kang and E. M. Yeatman, *Appl. Energy* **262**, 114496 (2020).
- <sup>11</sup>C. Wang, Y. Ji, S.-K. Lai, Y. Liu, Y. Hao, G. Li, C. Wang, and G.-L. Wen, *Nano Energy* **114**, 108630 (2023).
- <sup>12</sup>D. Zhu, M. J. Tudor, and S. P. Beeby, *Meas. Sci. Technol.* **21**(2), 022001 (2009).
- <sup>13</sup>H. Chen, C. Xing, Y. Li, J. Wang, and Y. Xu, *J. Sustainable Energy Fuels* **4**(3), 1063 (2020).
- <sup>14</sup>S. Shahari, Ph.D. thesis, University of Calgary (2020).
- <sup>15</sup>S. Niu and Z. L. Wang, *Nano Energy* **14**, 161 (2015).
- <sup>16</sup>Z. L. Wang, *ACS Nano* **7**(11), 9533 (2013).
- <sup>17</sup>S. Kumar, R. K. Jha, U. Chitnis, S. Singh, J. K. Anand, S. K. Roy, and A. Goswami, *J. Vac. Sci. Technol. B* **41**(3), 032806 (2023).
- <sup>18</sup>W. Liu, Z. Wang, G. Wang, G. Liu, J. Chen, X. Pu, Y. Xi, X. Wang, H. Guo, C. Hu, and Z. L. Wang, *Nat. Commun.* **10**(1), 1426 (2019).
- <sup>19</sup>M. P. Mahmud, J. Lee, G. Kim, H. Lim, and K.-B. Choi, *Microelectron. Eng.* **159**, 102 (2016).
- <sup>20</sup>L. Cheng, Q. Xu, Y. Zheng, X. Jia, and Y. Qin, *Nat. Commun.* **9**(1), 3773 (2018).
- <sup>21</sup>X. He, H. Guo, X. Yue, J. Gao, Y. Xi, and C. Hu, *Nanoscale* **7**(5), 1896 (2015).
- <sup>22</sup>L. Niu, X. Miao, Y. Li, X. Xie, Z. Wen, and G. Jiang, *Nanoscale Res. Lett.* **15**, 181 (2020).
- <sup>23</sup>M. Salauddin, S. M. S. Rana, M. T. Rahman, M. Sharifuzzaman, P. Maharjan, T. Bhatta, H. Cho, S. H. Lee, C. Park, K. Shrestha *et al.*, *Adv. Funct. Mater.* **32**(5), 2107143 (2022).
- <sup>24</sup>I. Z. Hossain, A. Khan, and G. Hossain, *Energies* **15**(15), 5541 (2022).
- <sup>25</sup>Q. Shi, H. Wu, H. Wang, H. Wu, and C. Lee, *Adv. Energy Mater.* **7**(22), 1701300 (2017).
- <sup>26</sup>X. Cao, Y. Xiong, J. Sun, X. Zhu, Q. Sun, and Z. L. Wang, *Adv. Funct. Mater.* **31**(33), 2102983 (2021).
- <sup>27</sup>M.-G. Kang, W.-S. Jung, C.-Y. Kang, and S.-J. Yoon, *Actuators* **5**, 5 (2016).
- <sup>28</sup>J. J. Ruan, R. A. Lockhart, P. Janphuang, A. V. Quintero, D. Briand, and N. de Rooij, *IEEE Trans. Instrum. Meas.* **62**(11), 2966 (2013).
- <sup>29</sup>S. Zhao, H. Fu, K. Ma, and J. Ma, *IEEE Sensors Journal* **18**(22), 9286 (2018).
- <sup>30</sup>D. Hong, Y.-M. Choi, and J. Jeong, *Rev. Sci. Instrum.* **89**(6), 065110 (2018).

- <sup>31</sup>M. O. Shaikh, Y.-B. Huang, C.-C. Wang, and C.-H. Chuang, *Micromachines* **10**(7), 438 (2019).
- <sup>32</sup>H. Zhang, Y. Lu, A. Ghaffarinejad, and P. Bassett, *Nano Energy* **51**, 10 (2018).
- <sup>33</sup>S. W. Chen, X. Cao, N. Wang, L. Ma, H. R. Zhu, M. Willander, Y. Jie, and Z. L. Wang, *Adv. Energy Mater.* **7**(1), 1601255 (2017).
- <sup>34</sup>S. S. K. Mallineni, H. Behlow, R. Podila, and A. M. Rao, *Nanotechnol. Rev.* **7**(2), 149 (2018).
- <sup>35</sup>A. Sharma and P. Agarwal, *J. Vib. Control* **29**(3–4), 942 (2023).
- <sup>36</sup>N. Wang and W. Lin, *Neurocomputing* **179**, 110 (2016).
- <sup>37</sup>L. Liu, *Electrostatic Generation and Control on Textiles* (North Carolina State University, 2010).
- <sup>38</sup>J. Chen, Y. D. Lim, Y. Zhao, J. Chen, B. Yang, Z. Wu, and Y. Li, *ACS Appl. Electron. Mater.* **3**(1), 476 (2021).
- <sup>39</sup>P. Lv, Z. Dong, X. Dai, and X. Qiu, *ACS Appl. Polym. Mater.* **1**(10), 2597 (2019).
- <sup>40</sup>Y. Xie, Z. Wang, X. Ren, M. F. Antwi-Afari, Y. Wang, H.-Y. Mi, B. Yang, C. Liu, and C. Shen, *Compos. Sci. Technol.* **237**, 110014 (2023).
- <sup>41</sup>G. Min, Y. Xu, P. Cochran, N. Gadegaard, D. M. Mulvihill, and R. Dahiya, *Nano Energy* **83**, 105829 (2021).